Malaysian Journal of Catalysis
http://mjcat.utm.my/
MJCat Research Article

Catalytic deoxygenation of *Reutealis trisperma* oil over Al-MCM-41 derived from red mud

Reva Edra Nugraha[1]*, Afna Agata Zendasary[2], Suprapto Suprapto[2], Abdul Aziz[2], Holilah Holilah[3], Didik Prasetyoko[2]*

[1]*Department of Chemical Engineering, Faculty of Engineering, Universitas Pembangunan Nasional "Veteran" Jawa Timur, Surabaya, East Java, 60294, Indonesia*
[2]*Department of Chemistry, Faculty of Science and Data Analytics, Institut Teknologi Sepuluh Nopember, Keputih, Sukolilo, Surabaya, 60111, Indonesia*
[3]*Research Center for Biomass and Bioproducts, National Research and Innovation Agency of Indonesia (BRIN), Cibinong, 16911, Indonesia*

**Corresponding Author: reva.edra.tk@upnjatim.ac.id; didikp@chem.its.ac.id*

Article history:
Received 29 April 2024
Accepted 06 August 2024

ABSTRACT

The Al-MCM-41 was successfully synthesized from red mud as silica and alumina source. The synthesis process involved a two-step hydrothermal method using CTABr as the mesopore template. The XRD analysis shows an amorphous structure characteristic of Al-MCM-41 with uniform hexagonal pore structure. The resulting Al-MCM-41 had a high surface area of 461.37 m^2/g with the high pore volume of 0.41 cc/g. Morphologically, the Al-MCM-41 catalyst displayed agglomerated small crystallites with particle sizes ranging from 0.6 to 1.4 μm. Elemental analysis showed the catalyst comprised Al, Si, Fe, and O elements, with percentages of 5.45%, 39.61%, 2.72%, and 49.09%, respectively. The catalyst was used in the catalytic deoxygenation of *Reutealis trisperma* oil to produce diesel-range hydrocarbon. Furthermore, GC-MS analysis of the liquid product demonstrated a selectivity of 48.5% for hydrocarbons and 28.14% of aromatic.

Keywords: *red mud, Al-MCM-41, deoxygenation, hydrocarbon*

| eISSN 0128-2581 |

1. INTRODUCTION

The aluminum industry's development has led to several significant challenges, particularly in waste management. A notable issue is the production of red mud (RM) during the alumina production process using the Bayer method, resulting in brownish-red solid waste. Statistical data indicates that the global abundance of RM reached 4 billion tonnes in 2019, with an estimated annual increase of up to 150 million tonnes [1–4]. Red mud, which has a pH of roughly 10–13.3, has significant alkaline qualities. The accumulation of moist mud in rivers or ponds raises the pH of the water system since it is an alkaline waste. If red mud is directly released into the environment without being treated, it must be stored properly across a wide region to avoid negative effects on the soil and water [5]. Red mud accumulation's negative effects on the environment might be mitigated by using it as a source of minerals for chemical synthesis. Red mud contains several metal oxides like Al2O3, CaO, Fe2O3, SiO2, TiO2 etc [6,7]. Researchers have explored various applications of red mud, such as using it as a precursor in zeolite synthesis [7,8], mesoporous alumina [9], mesoporous aluminosilicate [10], concrete raw materials [11], road materials [12] etc. In previous study, thermal and chemical treatments were performed to remove impurities from the red mud before its use in chemical synthesis. In the synthesis of ZSM-5, red mud is treated with NaOH to eliminate iron species that could compromise zeolite purity [13]. Some researchers have used calcination to transform the crystalline phase of red mud into an amorphous form [14]. Adding citric acid decreased the pH and total alkalinity of red mud by enhancing the solubility of Na, Ca, and Al [15].

The synthesis of acid catalysts like Al-MCM-41 has practical applications in catalytic deoxygenation reactions. Al-MCM-41's unique characteristics, including its mesoporous structure and high acid sites, enable it to significantly enhance hydrocarbon production from triglycerides. In the context of biofuel production, the catalytic deoxygenation reaction plays a crucial role. This reaction requires a catalyst to remove oxygen content from fatty acids while also inhibiting hydrocracking reactions, thereby ensuring the formation of hydrocarbons with appropriate chain lengths [16–18]. The utilization of a catalyst in the deoxygenation reaction is expected to increase

biofuel products within the C11-C18 range while reducing carbonyl compounds. The previous study reported that employing an acid catalyst with high Lewis acid sites can boost hydrocarbon products (C11-C18) while decreasing carbonyl compounds in vegetable oil [16]. Additionally, studies have indicated that the presence of Fe content in the catalyst can inhibit the C-C bond cracking reaction in the target hydrocarbon range (C11-C18), thereby enhancing catalytic activity and hydrocarbon selectivity [19]. Besides catalyst design, selecting the appropriate feedstock is also crucial for biofuel production. Non-edible oil is preferred as a feedstock over edible oil due to competition in the food sector. Reutealis trisperma is a promising non-edible biodiesel plant, known for its high seed production capacity and oil content. Additionally, it can thrive in unfavorable environmental conditions [20].

In this research, the Al-MCM-41 catalyst was synthesized using red mud as a source of alumina and silica. The catalytic activity of Al-MCM-41 is being investigated through the deoxygenation reaction of Reutealis trisperma oil

2. EXPERIMENTS

2.1 Materials

Red mud (bauxite waste) acquired from Bintan Island, Riau, Indonesia, Sodium Hydroxide (NaOH Merck, 99%), LUDOX Colloidal Silica (Sigma Aldrich 30% silica), Hexadecyltrimethylammonium bromide (CTAB, Sigma Aldrich 98%), Citric Acid ($C_6H_8O_7$. H_2O, Merck 99%), n-hexane, distilled water and N_2 Ultra High Purity (UHP) gas.

2.2 Preparation of Red Mud

The red mud (RM) sample from the Bintan Islands was ground and sieved through a 125-mesh screen to achieve a finer grain size to increase the reactivity. The silica (SiO_2) in red mud was dissolve by mixing 100 mL (1 M) citric acid with 1 g red mud and stirred for 24 h. Subsequently, the mixture of red mud and citric acid (referred to as RCA) underwent centrifugation to separate the sediment. The resulting brown precipitate was then subjected to drying in an oven set at 80°C.

2.3 Synthesis of Al-MCM-41

The synthesis of Al-MCM-41 was conducted via the hydrothermal method, employing a molar composition of 10 Na_2O : 100 SiO_2 : 2 Al_2O_3 : 1800 H_2O. The molar ratio of SiO_2 to CTABr was 3.85. The RCA was used as silica source and alumina. Initially, 1.6603 g of NaOH dissolved in 19.4186 g of distilled water in a PP bottle and stirred for 30 minutes. Then, 0.7196 g of RCA was added as the silica and alumina source to the mixture. Subsequently, Ludox was gradually introduced along with distilled water to prevent clumping, and stirring continued for 8 h. After completion, the gel mixture was left to age for 6 h at 70 ℃. The first hydrothermal process occurred at 80 ℃ for 12 h following the aging process. CTABr was slowly incorporated into the mixture and stirred until it had a slurry texture. The second hydrothermal process took place in an autoclave at 150 ℃ for 24 h. The resulting solid was washed with distilled water until neutral (pH = 7) and then dried at 60 ℃ for 24 h. Subsequently, the dry powder underwent calcination in a tubular furnace at 550 °C (2 ℃/minute) under a flow of N_2 gas for 1 h, followed by 6 h under airflow.

2.4 Catalyst Characterization

The wide X-ray Diffraction (XRD) characterization utilizing a PHILIPS-binary XPert with MPD diffractometer with Cu K radiation operating at 30 mA and 40 kV was used to examine the phase transformation of red mud to Al-MCM-41. The low XRD was performed with Bruker type D2 Phaser using KFL Cu 2K radiation at 10 mA and 30 kV to analyze the pore uniformity in Al-MCM-41. Shimadzu Instrument Spectrum One 8400S's Fourier Transform Infra-Red (FTIR) within range of 400-1400 cm^{-1} measurement was used to examine the functional group of catalyst. The specific surface area was assessed using the Brunauer–Emmet–Teller (BET) method through N_2 Adsorption-Desorption analysis. This analysis was conducted at 363 K utilizing a Quantachrome Touchwin v1.11 instrument.

2.5 The Catalytic Deoxygenation

The deoxygenation process involved 10 g *Reutealis trisperma* oil (RTO) and 0.3 g of catalyst placed in a three-neck flask connected to distillation equipment and a heating mantle. The reaction proceeded at approximately 350 ℃ for 4 h. After completion of the reaction, the catalyst and residue were weighed and washed with n-hexane for catalyst reuse. The resulting deoxygenation product was weighed and subjected to analysis using Gas Chromatography-Mass Spectrometry (GC-MS). Subsequently, the Degree of Deoxygenation (DD) (Eq. 1), conversion (Eq. 2), selectivity (Eq. 3) and yield (Eq. 4) of the deoxygenation product were calculated.

$$Degree\ of\ deoxygenation\ (DD) = \left[1 - \left(\frac{\%FA\ in\ liquid\ product}{\%FA\ in\ reactant}\right)\right] x100\% \quad \text{Eq. 1}$$

$$Conversion\ (\%) = \left(\frac{\frac{weight\ of\ initial\ reactant - weight\ of\ final\ reactant}{weight\ of\ initial\ reactant}}{}\right) x100\% \quad \text{Eq. 2}$$

$$Selectivity = \frac{(peak\ area\ of\ desired\ product)}{(peak\ area\ of\ total\ product)}\ x\ 100\% \quad \text{Eq. 3}$$

$$Liquid\ yield\ (\%) = \left(\frac{weight\ of\ liquid\ product}{weight\ of\ initial\ reactant}\right) x100\% \quad \text{Eq. 4}$$

3. RESULTS AND DISCUSSION

3.1 Red Mud Pre-Treatment

This citric acid treatment serves to dissolve the mineral content present in red mud. According to research conducted by Kalsen et al. (2019), it demonstrates that the reduction in silica (Si) content achieved through citric acid has shown an increase compared to HCl [21]. XRD analysis was conducted to determine the crystalline phase of the sample. According to the XRD pattern depicted in Fig. 1, no notable difference was observed between RM and RCA. The diffractograms display peaks corresponding to Gibbsite ($Al(OH)_3$) at 2θ = 18.05° and 18.10°, hematite (Fe_2O_3) at 2θ = 24.62°, 35.75°, and 45.33°, and quartz (SiO_2) at 2θ = 26.39° and 26.60° [7]. A noticeable difference in peak intensity between the two diffractograms indicates crystallization within the sample. Specifically, there is a reduction in the intensity of the quartz peak in the activated red mud diffractogram, suggesting a successful separation of quartz (SiO_2) from the red mud.

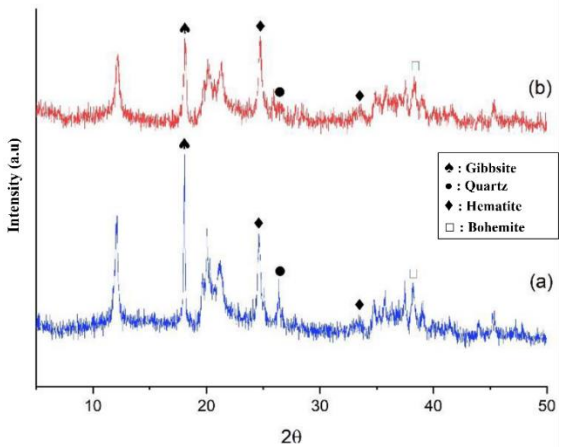

Fig. 1. Diffraction pattern of a) RM and b) RCA

The findings from the XRD analysis are further supported by the FTIR characterization of RM and RCA. In Fig. 2, the RM and RCA shows similar absorption band of Si-O, Al-O and Fe-O. The peaks are observed at wave numbers 462 – 468 cm^{-1} and 549 – 540 cm^{-1}, indicating bonds related to (Fe^{3+} - O^{2-}) which correspond to the presence of hematite (Fe_2O_3). Additionally, peaks at wave numbers 999 – 1000 cm^{-1} suggest the presence of Si-O bonds from quartz, while peaks at 874 cm^{-1}, 712 cm^{-1}, and 628 cm^{-1} indicate the bond (Al^{3+} - O^{2-}) from Gibbsite ($Al(OH)_3$) [22,23].

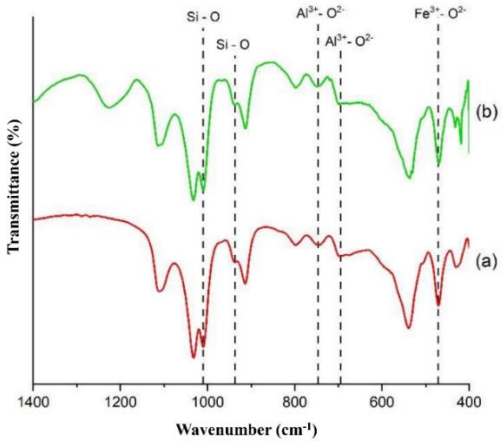

Fig. 2. FTIR spectra of a) RM and b) RCA

The results from N_2 adsorption-desorption analysis confirm that red mud is a non-porous material. The isotherm graph for both RM and RCA samples, shown in Fig. 3a, exhibits a type II isotherm according to the IUPAC classification. The type II isotherm observed in both RM and RCA indicates that they are non-porous materials [24–26]. This conclusion is further supported by the absence of hysteresis, which typically signifies the presence of condensed adsorbate liquid between non-porous particles [27]. The similarity between the two isotherms without prominent differences suggests that there is no structural change between red mud (RM) and red mud activated by citric acid (RCA).

Table 1. The textural properties of RM, RCA and Al-MCM-41

Sample	Surface area(m^2/g)			Pore volume (cc/g)			d (nm)
	S_{BET}[a]	S_{micro}[b]	S_{meso}[b]	V_{total}[d]	V_{micro}[b]	V_{meso}[c]	
RM	61.81	34.89	26.92	0.26	0.2	0.24	42.79
RCA	66.53	34.84	31.7	0.25	0.2	0.23	11.4
Al-MCM-41	461.73	377.38	84.35	0.41	0.04	0.37	2.5

[a]S_{BET} by BET method
[b]S_{micro},S_{meso} and V_{micro} by t-plot method
[c]V_{meso} by BJH desorption
[d]V_{total}= V_{micro}+V_{meso}

The pore distribution of RM and RCA were shown in Fig. 3b. RM shows the higher pore diameter of 42.79 nm, meanwhile the RCA shows the lower pore diameter of 11.4 nm. As shown in Table 1, the RM sample has a total surface

area of 61.81 m^2/g and a total pore volume of 0.26 cc/g, while the RCA sample exhibits an increased total surface area of 66.53 m^2/g and a total pore volume of 0.25 cc/g.

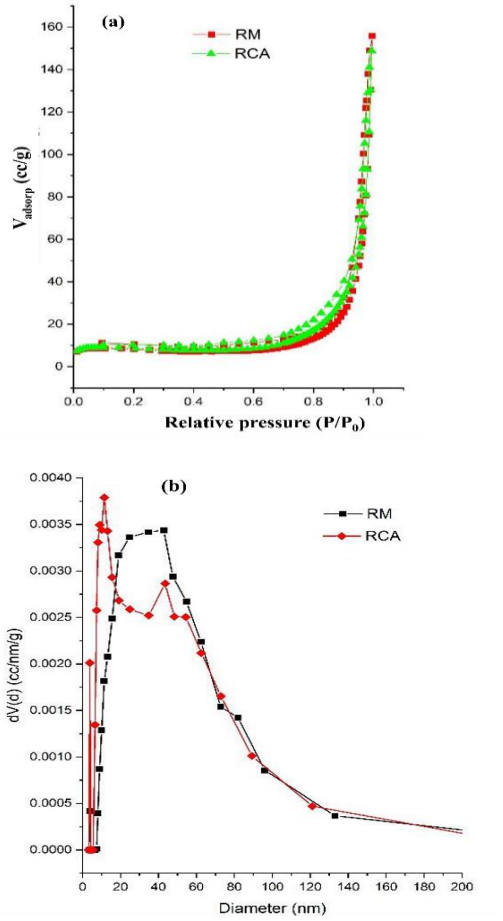

Fig. 3. The N_2 adsorption-desorption of isotherm and pore size distribution of RM and RCA

3.2 FTIR

The wide-angle XRD analysis results, as depicted in Fig. 4a reveal a broad peak at around $2\theta = 23°$, indicating the formation of an amorphous structure from silica [28]. Fig. 4b, displaying the low-angle XRD pattern of the Al-MCM-41 catalyst, shows a strong peak at $2\theta = 2.2°$ corresponding to the (100) plane, along with two weaker peaks at $2\theta = 3.5°$ - 4.2° related to the (110) and (200) plane reflections [29,30]. These peaks collectively suggest the formation of a well-structured mesoporous material consistent with the hexagonal structure of MCM-41[31]. The strong and sharp peak of the (100) plane further indicates good crystallization of the mesoporous structure [32].

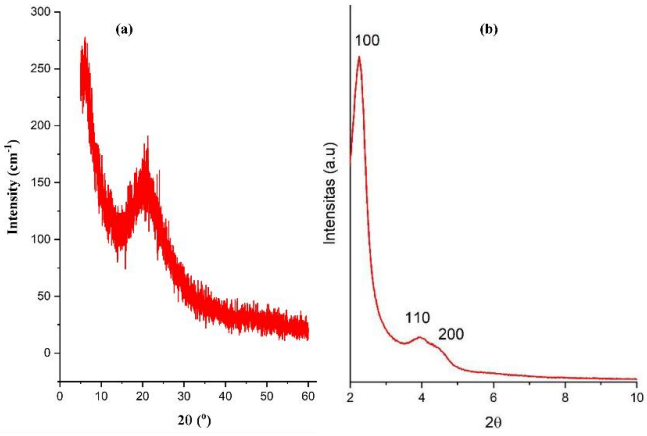

Fig. 4. The wide a) and low angle b) XRD analysis of Al-MCM-41

The FTIR spectra of Al-MCM-41 was depicted in Fig. 5 reveal a peak at a wavenumber of 457 cm^{-1} corresponding to the Si-O vibration of TO_4 [33]. Additionally, the peak at 798 cm^{-1} signifies the bending vibration of the Si-O-Si group [34]. The peak observed at the wavenumber of 1100 cm^{-1} corresponds to the internal asymmetric stretching vibration of the T-O-T bond, where T can be Si or Al [35]. The peak in the range of 950-970 cm^{-1} is typically associated with Si-OH or $Si\text{-}OM^+$ vibrations [33]. Additionally, the wavenumber 1220 cm^{-1} represents the external asymmetric stretching vibration of Si-O [36].

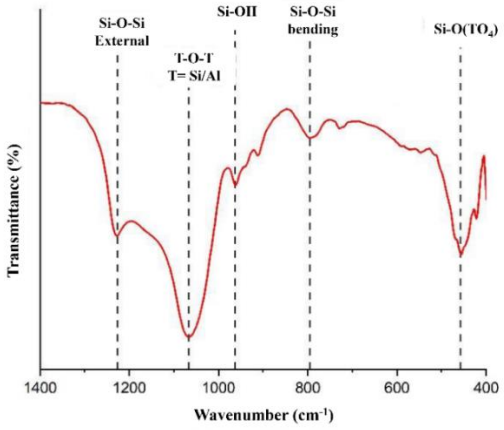

Fig. 5. FTIR spectra of Al-MCM-41

According to IUPAC, the Al-MCM-41 isotherm depicted in Fig. 6a is classified to type IV isotherm with type H1 hysteresis [37,38]. The Al-MCM-41 catalyst's isotherm shows a typical mesoporous material with hysteresis at P/Po = 0.4 – 1 [39]. The hysteresis curve is associated with the secondary capillary condensation process, which fills the pores at P/Po < 1 in mesoporous materials [40,41]. The Al-MCM-41 catalyst exhibits an H1 hysteresis type, indicating that the sample comprises plate-like particles and pores resembling gaps. This type of hysteresis is often observed in catalyst samples synthesized from clay, where the pores

resemble gaps [42]. The analysis of pore distribution in Al-MCM-41 using the BJH method (Fig. 6b) indicates that the catalyst's pore diameter ranges from 1.8 to 5.5 nm. According to Table 1, the Al-MCM-41 catalyst has a total surface area of 461.73 m^2/g and a total pore volume of 0.41 cc/g. This signifies an increase in the surface area of RM and RCA on Al-MCM-41, suggesting improved catalytic activity in deoxygenation reactions.

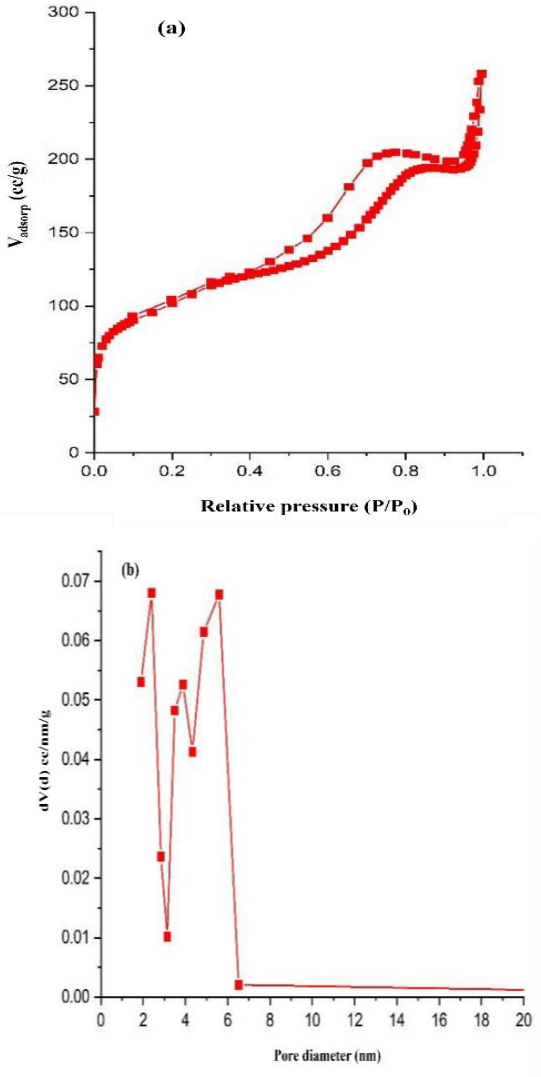

Fig. 6. a) The N_2 adsorption-desorption of isotherm and b) pore size distribution of Al-MCM-41

The SEM-EDX analysis revealed the morphology and elemental composition of the samples. The SEM profile depicted in Fig. 7 indicates that red mud has a particle size ranging from 0.4 to 1.3 µm, with irregular particle shapes. Some particles appear spherical and agglomerated [43]. On the other hand, the morphology of Al-MCM-41 shows small crystals agglomerating into larger aggregates [17]. The particle size of Al-MCM-41 ranges from 0.6 to 1.4 µm. The EDX analysis results indicate the presence of Al, Si, Fe, and O elements in both red mud and the Al-MCM-41 catalyst, as shown in Table 2. From the table, it is evident that there was a decrease in Al content and an increase in Si content from red mud to Al-MCM-41. This change is attributed to the lower molar ratio of Al compared to Si during the synthesis of Al-MCM-41, resulting in a higher Si content in the catalyst. Similarly, there was a decrease in Fe content in Al-MCM-41 compared to red mud. This reduction in Fe content is due to the pre-treatment of the red mud material before its use in catalyst synthesis [9].

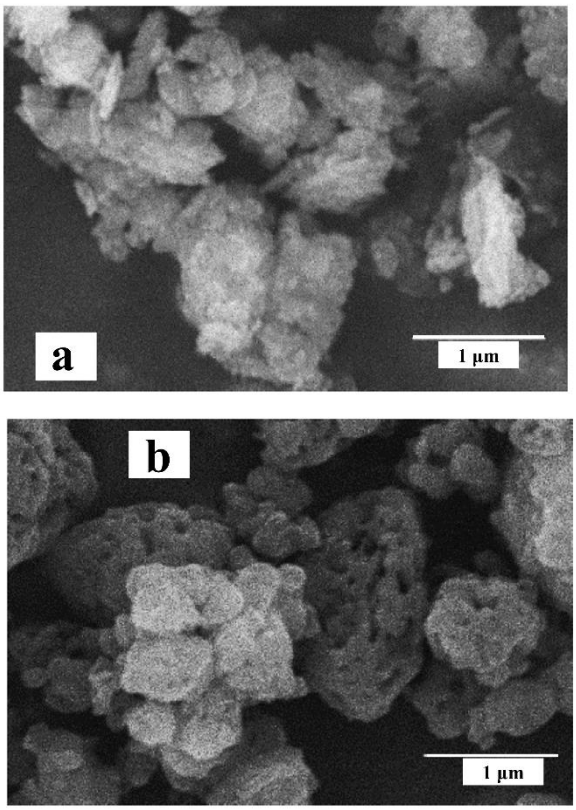

Fig. 7. The SEM images of a) RM and b) Al-MCM-41

Table 2. The EDX analysis of RM and Al-MCM-41

Element	%weight		%atom	
	RM	Al-MCM-41	RM	Al-MCM-41
Al	22.90	5.45	17.31	4.16
Si	12.95	39.61	9.40	28.99
Fe	8.01	2.72	2.93	1.00
O	54.22	49.09	69.10	63.06

3.3 Catalytic Activity

The catalytic activity was tested in the deoxygenation reaction of *Reutealis trisperma* oil. The deoxygenation reaction was carried out for 4 h at 350°C with a N_2 gas flow. In this catalytic activity test, the GC-MS instrument was utilized to perform qualitative and quantitative analysis on the deoxygenation process product. The conversion, yield and degree of deoxygenation of liquid product obtained from

different catalysts was shown in Table 3. The deoxygenation reaction of *Reutealis trisperma* oil resulted in the conversion of reactants into liquid (bio-oil), gas (CO and CO_2) and coke. According to Table 3, using RCA as a catalyst yielded the highest conversion rate at 64.45%, with a liquid yield of 33.44%. On the other hand, the Al-MCM-41 catalyst achieved a conversion rate of 45.4% with a liquid yield of 17.99%. The highest hydrocarbon selectivity was observed when using the Al-MCM-41 catalyst at 48.50%. Interestingly, even without a catalyst, the reaction showed good selectivity at 45.78%. However, the use of a catalyst notably increased the amount of oil converted and provided a higher liquid yield. This underscores the influence of acid sites and mesoporosity on the catalyst in promoting the conversion of *Reutealis trisperma* oil into hydrocarbons [44].

Table 3. Conversion, yield and degree of deoxygenation of liquid product

Catalysts	Conversion (%)	Yield (%)	Degree of Deoxygenation
Blank	41.8	9.24	45.78
RM	45.1	11.7	34.00
RCA	64.45	33.44	14.89
Al-MCM-41	45.5	17.99	48.50

The GC-MS analysis of deoxygenation liquid products reveals several data points, including the distribution of compounds from oil and the distribution of carbon chains. Figure 8, illustrates the composition of the liquid deoxygenation product, which includes hydrocarbons, cyclic compounds, aromatics, carboxylic acids, and ketones. The catalytic activity of the sample is reflected in the selectivity of hydrocarbons and compounds containing oxygen. Specifically, the Al-MCM-41 catalyst demonstrates good hydrocarbon selectivity at 48.50%, with a carboxylic acid selectivity that is 12.74% lower compared to other reactions. This lower selectivity for carboxylic acids suggests a reduction in the oxygen content of the deoxygenation product, indicating the effective conversion of oxygen-containing compounds into hydrocarbons. The activity test for the Al-MCM-41 catalyst also revealed an aromatic compound selectivity of 28.14%, which is attributed to the Bronsted acid site. In biofuel production via deoxygenation reaction, the goal is to reduce the oxygen component. Aromatic compounds can lower the freezing point, reduce the energy released during combustion, and decrease oil viscosity [45]. Therefore, achieving good hydrocarbon and aromatic selectivity is a desirable outcome in this research. The selectivity observed corresponds to the degree of deoxygenation achieved by RCA, which is 83.94% compared to the blank reaction (91.71%), RM (93.15%), and the highest with Al-MCM-41 (93.17%). The degree of deoxygenation is directly related to the reduction in the concentration of fatty acids in the liquid deoxygenation product, thereby impacting its composition [46].

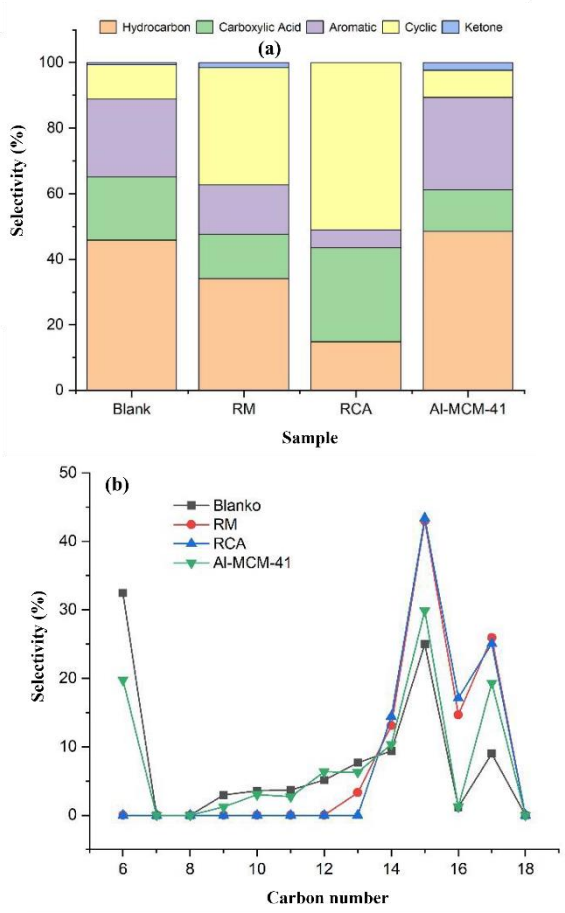

Fig. 8. Hydrocarbon distribution from catalytic deoxygenation reaction of *Reutealis trisperma* oil

The deoxygenation process results in oxygen-free hydrocarbons with one fewer carbon atom than the original fatty acid (C_{16-18}). These hydrocarbons are categorized into short carbon chains (C_{6-10}) and long carbon chains (C_{11-17}). Fig. 8b illustrates the carbon chain distribution, showing that when using Al-MCM-41 as the catalyst, the deoxygenation product comprises 24% short carbon chains (C_{6-10}) and 76% long carbon chains (C_{11-17}), with the primary product being (C_{15}+C_{17}) at 49.2%. This indicates successful deoxygenation of RTO with this catalyst. In the deoxygenation of *Reutealis trisperma* oil using the Al-MCM-41 catalyst, there is a significant formation of short-chain hydrocarbons (C_{6}-$_{10}$). This formation of short-chain hydrocarbon products is believed to result from a secondary hydrocracking reaction. The catalyst's characteristics, especially a higher concentration of Brønsted acid compared to Lewis acid, can indeed trigger hydrocracking reactions, resulting in a higher yield of short-chain hydrocarbons (C_{8-10}) [47,48]. The catalyst's characteristics, especially a higher concentration of Brønsted acid compared to Lewis acid, can indeed trigger hydrocracking reactions, resulting in a higher yield of short-chain hydrocarbons (C_{8-10}). This is because Brønsted acid sites are known to promote hydrocracking reactions, which break down larger hydrocarbons into smaller ones, thus favoring the production of shorter carbon chain compounds

[16]. This is because Brønsted acid sites are known to promote hydrocracking reactions, which break down larger hydrocarbons into smaller ones, thus favoring the production of shorter carbon chain compounds.

4. CONCLUSION

The Al-MCM-41 catalyst derived from red mud has been successfully synthesized. This catalyst boasts a substantial total surface area of 461.73 m^2/g, with a mesopore surface area measuring 84.35 m^2/g and a mesopore volume of 0.37 cc/g. Featuring a pore diameter of 2.5 nm, the morphology of Al-MCM-41 reveals the agglomeration of small crystals into larger aggregates, presenting a particle size range of 0.6 – 1.4 μm. The elemental composition showcases the presence of Al (5.45%), Si (39.61%), Fe (2.72%), and O (49.09%). In catalytic tests involving the deoxygenation reaction of *Reutealis trisperm*a oil, the Al-MCM-41 catalyst demonstrated a remarkable hydrocarbon selectivity of 48.5%, alongside a notably low carboxylic acid selectivity of 12.74% compared to alternative catalysts utilized in similar reactions.

ACKNOWLEDGEMENTS

The authors acknowledge the Ministry of Education, Culture, Research, and Technology of Republic Indonesia under PDUPT research grant with contract number 1209/PKS/ITS/2023 for funding the research and Universitas Pembangunan Nasional “Veteran” Jawa Timur under Penelitian Dasar Lanjutan scheme with contract number of SPP/130/UN.63.8/LT/V/2024 for funding the research.

REFERENCES

[1] P.B. Cusack, M.G. Healy, P.C. Ryan, I.T. Burke, L.M.T. O’ Donoghue, É. Ujaczki, R. Courtney, 179 (2018) 217–224.https://doi.org/10.1016/j.jclepro.2018.01.092.

[2] K. Evans, (2016) 316–331. https://doi.org/10.1007/s40831-016-0060-x.

[3] P.S. Reddy, N.G. Reddy, V.Z. Serjun, B. Mohanty, S.K. Das, K.R. Reddy, B.H. Rao, , Springer Netherlands, 2021. https://doi.org/10.1007/s12649-020-01089-z.

[4] L. Wang, G. Hu, F. Lyu, T. Yue, H. Tang, H. Han, Y. Yang, R. Liu, W. Sun, (2019). https://doi.org/10.3390/min9050281.

[5] E.P. Ramdhani, E. Santoso, H. Holilah, R.E. Nugraha, H. Bahruji, S. Suprapto, A.A. Jalil, N. Asikin-Mijan, S. Akhlus, D. Prasetyoko, (2023) 31989–31999. https://doi.org/10.1039/d3ra05910c.

[6] H. Jahromi, F.A. Agblevor, (2018) 1–12. https://doi.org/10.1016/j.apcatb.2018.05.008.

[7] H. Tehubijuluw, R. Subagyo, M.F. Yulita, R.E. Nugraha, Y. Kusumawati, H. Bahruji, A.A. Jalil, H. Hartati, D. Prasetyoko, (2021) 1–17.

[8] C. Belviso, A. Kharchenko, E. Agostinelli, F. Cavalcante, D. Peddis, G. Varvaro, N. Yaacoub, S. Mintova, (2018) 24–29. https://doi.org/10.1016/j.micromeso.2018.04.038.

[9] E.P. Ramdhani, T. Wahyuni, Y.L. Ni’mah, Suprapto, D. Prasetyoko, (2018) 337–343. https://doi.org/10.22146/ijc.25108.

[10] F. Wulandari, E.P. Ramdhani, Y.L. Ni’mah, A.A. Dawam, D. Prasetyoko, (2018) 580–586. https://doi.org/10.22146/ijc.25184.

[11] W.C. Tang, Z. Wang, S.W. Donne, M. Forghani, Y. Liu, (2019) 120802. https://doi.org/10.1016/j.jhazmat.2019.120802.

[12] J. Zhang, Z. Yao, K. Wang, F. Wang, H. Jiang, M. Liang, J. Wei, G. Airey, (2021) 121419. https://doi.org/10.1016/j.conbuildmat.2020.121419.

[13] R. Subagyo, H. Tehubijuluw, W.P. Utomo, H.D. Rizqi, Y. Kusumawati, H. Bahruji, D. Prasetyoko, (2022) 103754. https://doi.org/10.1016/j.arabjc.2022.103754.

[14] M. HM Ahmed, N. Batalha, Z.A. ALOthman, Y. Yamauchi, Y. Valentino Kaneti, M. Konarova, (2022) 132965. https://doi.org/10.1016/j.cej.2021.132965.

[15] X. Kong, M. Li, S. Xue, W. Hartley, C. Chen, C. Wu, X. Li, Y. Li, (2017) 382–390. https://doi.org/10.1016/j.jhazmat.2016.10.073.

[16] R.E. Nugraha, D. Prasetyoko, Hasliza Bahruji, Suprapto Suprapto, Nurul Asikin-Mijan, T. Prapti Oetami, A. Abdul Jalil, D.-V. N. Vo, Y. Hin Taufiq-Yap, (2021) 21885–21896. https://doi.org/10.1039/D1RA03145G.

[17] R.E. Nugraha, D. Prasetyoko, N. Asikin-Mijan, H. Bahruji, S. Suprapto, Y.H. Taufiq-Yap, A.A. Jalil, (2021) 110917. https://doi.org/10.1016/j.micromeso.2021.110917.

[18] K. de Sousa Castro, L. Fernando de Medeiros Costa, V.J. Fernandes, R. de Oliveira Lima, A. Mabel de Morais Araújo, M.C. Sousa de Sant’Anna, N. Albuquerque dos Santos, A.D. Gondim, (2020) 555–564. https://doi.org/10.1039/d0ra06122k.

[19] J. Zhong, Q. Deng, T. Cai, X. Li, R. Gao, J. Wang, Z. Zeng, G. Dai, S. Deng, (2021) 18–21. https://doi.org/10.1016/j.fuel.2021.120248.

[20] H. Hamim, M. Hilmi, D. Pranowo, D. Saprudin, L. Setyaningsih, (2017) 423–435. https://doi.org/10.3923/pjbs.2017.423.435.

[21] T.S. Atalay Kalsen, H.B. Karadağ, Y.R. Eker, I. Kerti, (2019) 482–496. https://doi.org/10.1007/s40831-019-00236-8.

[22] M. Mokhatr Mohamed, H. El-Faramawy, (2021) 120741. https://doi.org/10.1016/j.fuel.2021.120741.

[23] S. Singh, M.U. Aswath, R. Das Biswas, R. V. Ranganath, H.K. Choudhary, R. Kumar, B. Sahoo,

(2019) e00266. https://doi.org/10.1016/j.cscm.2019.e00266.
[24] I. V. Melnyk, V. V. Tomina, N. V. Stolyarchuk, G.A. Seisenbaeva, V.G. Kessler, (2021) 116301. https://doi.org/10.1016/j.molliq.2021.116301.
[25] P. Ehiomogue, I.I. Ahuchaogu, I.E. Ahaneku, (2022) 87–96. https://www.researchgate.net/publication/358271705.
[26] S.P. Rigby, 2020. https://doi.org/10.1007/978-3-030-47418-8.
[27] A. Milenković, I. Smičiklas, M. Šljivić-Ivanović, N. Vukelić, (2015) 2461–2465. https://doi.org/10.1134/S0036024415130269.
[28] N.T.T. Tran, Y. Uemura, S. Chowdhury, A. Ramli, (2016) 93–100. https://doi.org/10.1016/j.apcata.2015.12.021.
[29] M. Hachemaoui, C.B. Molina, C. Belver, J. Bedia, A. Mokhtar, R. Hamacha, B. Boukoussa, (2021) 1–17. https://doi.org/10.3390/catal11020219.
[30] H. Douba, O. Mohammedi, B. Cheknane, (2022) 569–582. https://doi.org/10.15255/kui.2022.001.
[31] S. Zhao, Z. Zhang, K. Zhu, J. Chen, (2017) 388–397. https://doi.org/10.1016/j.apsusc.2017.02.016.
[32] F. Mahmoudi, M.M. Amini, (2020) 101227. https://doi.org/10.1016/j.jwpe.2020.101227.
[33] S.T. Pham, M.B. Nguyen, G.H. Le, T.D. Nguyen, C.D. Pham, T.S. Le, T.A. Vu, (2021). https://doi.org/10.1016/j.chemosphere.2020.129062.
[34] M.S. Abdel Salam, M.A. Betiha, S.A. Shaban, A.M. Elsabagh, R.M. Abd El-Aal, F.Y. El kady, (2015) 49–57. https://doi.org/10.1016/j.ejpe.2015.02.005.
[35] Y. Yue, Y. Kang, Y. Bai, L. Gu, H. Liu, J. Bao, T. Wang, P. Yuan, H. Zhu, Z. Bai, X. Bao, (2018) 177–185. https://doi.org/10.1016/j.clay.2018.03.025.
[36] W.E. Rashwan, K.S. Abou-El-Sherbini, M.A. Wahba, S.A. Sayed Ahmed, P.G. Weidler, (2020) 2017–2029. https://doi.org/10.1007/s12633-019-00262-x.
[37] P. López-Aranguren, S. Builes, J. Fraile, A. López-Periago, L.F. Vega, C. Domingo, (2015) 104943–104953. https://doi.org/10.1039/c5ra20583b.
[38] G. Calzaferri, S.H. Gallagher, S. Lustenberger, F. Walther, D. Brühwiler, (2023) 127121. https://doi.org/10.1016/j.matchemphys.2022.127121.
[39] F.C.M. Silva, M.S. Lima, C.O.C. Neto, J.L.S. Sá, L.D. Souza, (2018) 159–167. https://doi.org/10.1007/s13399-017-0263-9.
[40] S. Mousa, K. Baron, R.S. Fletcher, S.P. Rigby, (2022) 130026. https://doi.org/10.1016/j.colsurfa.2022.130026.
[41] M.I.H.S. N., C. Panatarani, F. Faizal, C. Mulyana, I.M. Joni, (2023) 101637.
[42] O. Riski, D. Prasetyoko, D.K. Febrianti, Y.L. Nikmah, V.N. Iftitahiyah, H. Hartati, I. Qoniah, E. Santoso, (2019) 93–98. https://doi.org/10.11113/mjfas.v15n2019.1003.
[43] N. Deihimi, M. Irannajad, B. Rezai, (2018) 266–275. https://doi.org/10.1016/j.jenvman.2017.10.037.
[44] A. Veses, B. Puértolas, J.M. López, M.S. Callén, B. Solsona, T. García, (2016) 1653–1660. https://doi.org/10.1021/acssuschemeng.5b01606.
[45] S. Khan, A.N. Kay Lup, K.M. Qureshi, F. Abnisa, W.M.A. Wan Daud, M.F.A. Patah, (2019) 1–24. https://doi.org/10.1016/j.jaap.2019.03.005.
[46] D. Kubička, J. Horáček, M. Setnička, R. Bulánek, A. Zukal, I. Kubičková, (2014) 101–107. https://doi.org/10.1016/j.apcatb.2013.01.012.
[47] W. Trisunaryanti, I.I. Falah, D.R. Prihandini, M.F. Marsuki, (2019) 1523–1529. https://doi.org/10.31788/RJC.2019.1235297.
[48] Q. Tian, K. Qiao, F. Zhou, K. Chen, T. Wang, J. Fu, X. Lu, P. Ouyang, (2016) 7291–7297. https://doi.org/10.1021/acs.energyfuels.6b00978.